Journal of Power Sources 268 (2014) 443–450

Contents lists available at ScienceDirect

Journal of Power Sources

journal homepage: www.elsevier.com/locate/jpowsour

Coating TiVCr hydrogen storage alloy on the anode gas diffusion layer of proton exchange membrane fuel cells to improve performance

Sheng-Yu Fang [a], Rong-Hsin Huang [a], Lay Gaik Teoh [b], Kan-Lin Hsueh [d], Wen-Kai Chao [c], Du-Cheng Tsai [a], Tse-Ning Yang [a], Fuh-Sheng Shieu [a, *]

[a] Department of Materials Science and Engineering, National Chung Hsing University, Taichung 40227, Taiwan
[b] Department of Mechanical Engineering, National Pingtung University of Science and Technology, Pingtung 91201, Taiwan
[c] Department of Solar Engineering, AU Optronics Corporation, Taichung 40763, Taiwan
[d] Department of Energy Engineering, National United University, Miaoli 36003, Taiwan

HIGHLIGHTS

- A TiVCr alloy was coated onto the gas diffusion layer of PEMFCs for the first time.
- TiVCr coatings were coated on the gas diffusion layer by the sputtering technique.
- TiVCr coatings can be used as electrode materials for PEMFCs.
- MEA10 capacity was 43.67% higher than that of MEA0 at 65 °C operation temperature.

ARTICLE INFO

Article history:
Received 1 February 2014
Received in revised form
31 May 2014
Accepted 13 June 2014
Available online 20 June 2014

Keywords:
Hydrogen storage alloy
Gas diffusion layer
Proton exchange membrane fuel cells
Sputtering

ABSTRACT

In this study, a TiVCr hydrogen storage alloy was coated onto the anode gas diffusion layer (GDL) of proton exchange membrane fuel cells (PEMFCs) by direct-current sputtering to improve cell performance and durability. Scanning electron microscopy analysis indicated that the GDLs are well coated and that the TiVCr coating shows pyramidal protrusions. The single-cell performance of PEMFCs, in which the GDLs were coated with TiVCr hydrogen storage alloy as the anode, was investigated at cell temperatures of 25 and 65 °C (non-humidification and full-humidification conditions, respectively). The membrane-electrode assembly (MEA) with TiVCr hydrogen storage alloy-coated GDL (10 min sputtering time) exhibited optimal performance at 25 and 65 °C, with power densities 18.49% and 43.67%, respectively, higher than that without TiVCr hydrogen storage alloy coating. The MEA with the TiVCr-coated GDL obtained by 60 min of sputtering exhibited 90.6% greater durability under no-hydrogen flow conditions than the MEA without the TiVCr hydrogen storage alloy coating. These results demonstrate for the first time that GDLs coated with a hydrogen storage alloy such as TiVCr may be applied in PEMFCs to improve their performance and durability.

1. Introduction

Development of new alternative energy resources has become increasingly important in the 21st century. Proton exchange membrane fuel cells (PEMFCs), which use hydrogen as a fuel, have become a principal area of study in the field of renewable energy because of their high energy-conversion efficiency, high power density, low operating temperature, and near-zero pollutant emission [1–3]. Given these advantages, PEMFCs are expected to become broadly commercialized for use in transportation, residential, and portable device applications.

Considerable efforts have been devoted to the commercialization of PEMFCs. However, a number of key challenges have yet to be overcome. In recent years, improvements in the lightness, thinness, shortness, and overall size of PEMFCs have been achieved noticeably [4–6]. Hydrogen is vital in PEMFCs, but a highly pressurized hydrogen storage tank increases the PEMFC volume. In addition, the activity of hydrogen at the anode affect the performance of the membrane electrode assembly (MEA), particularly when using air as fuel. To solve this problem, developing an electrode material capable of storing hydrogen and exhibiting high activity with hydrogen is essential [7–10].

* Corresponding author. Tel.: +886 4 2285 4563; fax: +886 4 2285 7017.
E-mail address: fsshieu@dragon.nchu.edu.tw (F.-S. Shieu).

http://dx.doi.org/10.1016/j.jpowsour.2014.06.072
0378-7753/

TiVCr alloys with a body-centered cubic (BCC) crystal structure have recently attracted remarkable attention as multi-functional materials, not only because of their capability to absorb and desorb hydrogen under ambient conditions but also because of their high mechanical strength, excellent thermal stability, and good corrosion resistance; these characteristics are attributed to the high entropy effect of the material [11–16]. While numerous studies have reported the structural and mechanical properties of TiVCr alloy coatings [17–22], no study has yet focused on the application of TiVCr hydrogen storage alloy in PEMFCs.

This study investigates the feasibility of improving PEMFC performance and durability by coating the gas diffusion layer (GDL) in the anode with a TiVCr hydrogen storage alloy. The cell performance and characteristics of the MEA with and without the TiVCr-coated GDL are compared. The microstructure and morphology of the TiVCr coatings were characterized by X-ray diffractometry (XRD) and scanning electron microscopy (SEM). A single-cell durability test was performed at 0.6 V constant voltage under no-hydrogen flow conditions and 25 °C operating temperature. A polarization test was conducted at operating temperatures of 25 and 65 °C (non-humidification and full-humidification conditions, respectively) to investigate the effect of the TiVCr coating on the cell performance of the PEMFCs.

2. Experimental

2.1. Preparation of TiVCr-coated GDL and Pt/C catalyst

The GDL (SGL-10BA, SIGRACET®) was coated with a TiVCr thin film by direct current (DC) magnetron sputtering. The operating parameters of sputtering are listed in Table 1. The sputtering times for the TiVCr-coated GDL were 10, 30, and 60 min, and the resulting samples were labeled TiVCr-10 m, TiVCr-30 m, and TiVCr-60 m, respectively. Pt/C (20 wt.%) catalyst was synthesized by an impregnation method. The natural inorganic mineral, sodium montmorillonite (Nancor), was first used to disperse carbon black (CB; Vulcan XC-72, Cabot) in distilled water. The mixture was then ultrasonicated for 2 h to obtain a well-dispersed CB mixture. The platinum precursor ($H_2PtCl_6 \cdot 6H_2O$; Alfa Aesar, 99.95%), 10 mL of 1 M NaOH, and 10 mL of 99.8% methanol (EM-1001, ECHO, Chemical Co., Ltd.) were added to the mixture, which was then stirred at 80 °C for 4 h to disperse the Pt/C catalyst completely. The as-made Pt/C catalyst was filtered and dried in a vacuum oven at 100 Pa and 80 °C for 6 h.

2.2. Characterization of the TiVCr coatings

Microstructural characterization of the TiVCr alloy coatings was performed using a glancing-incidence (1°) X-ray diffractometer (MAC MXP III) operated at 40 kV and 30 mA with CuKα radiation (λ = 0.154 nm) at a sweeping angle of 2θ from 20° to 50° and 2° min^{-1} sweeping rate. Diffraction peaks were identified using JCPDS data files. The surface morphology of the carbon paper coated with TiVCr alloy thin films was examined by a field-emission scanning electron microscope (JEOL JEM-6700F). The chemical composition of the TiVCr-coated GDLs was estimated by an inductively coupled plasma-atomic emission spectrometry (ICP-AES) system (ICAP 9000, Jarrell-Ash, USA). The contact angle of water on the TiVCr-coated GDLs was measured using the sessile drop method by a Fat 200 contact angle system.

Table 1
Sputtering parameters of the TiVCr coatings on the GDLs.

Target	TiVCr
Substrate	Carbon paper (SGL-10BA)
Base pressure	1.0×10^{-5}
Working pressure	5.0×10^{-3}
DC power	250 W
Ar	50 sccm
Working distance	5 cm (holder location)
Sputtering time	10, 30, 60 min
Operation temperature	Room temperature

2.3. Evaluation of the PEMFC durability

After cell activation for 30 cycles, the hydrogen and oxygen flow rates were set to 0 and 50 sccm. The variation in current density as a function of time at a constant voltage of 0.6 V was measured using a fuel cell test station. Data were collected starting from zero hydrogen flow rate, and the test was stopped when the current density decreased to 0.02 A cm^{-2}.

2.4. Measurement of polarization curves

Certain amounts of 20 wt.% Pt/C catalyst, 5 wt.% Nafion solution (Dupont®), and alcohol (98%, Aldrich) were mixed for 2 h using an ultrasonicator. This mixture was sprayed onto the TiVCr-10 m, TiVCr-30 m, and TiVCr-60 m samples, which were then used as anodes As-received GDL substrate without the TiVCr coating was prepared using a similar method and used as a cathode. A Nafion 112 membrane (Dupont®) was sequentially pretreated with 5% H_2O_2 (Aldrich), DI water, and 1.0 M H_2SO_4 (Aldrich) at 80 °C for 1 h. The Nafion 112 membrane was sandwiched between the anode and the cathode and then hot-pressed under 20 kgf cm^{-2} at 135 °C for 3 min. The Pt loading at both the anode and the cathode was 0.4 mg cm^{-2}, and the effective area of the MEA was 5 cm^2. The anodes of MEA samples with TiVCr-10 m, TiVCr-30 m, and TiVCr-60 m GDLs, which were combined with the Nafion membrane and cathode, were labeled MEA10, MEA30, and MEA60, respectively. The as-received GDL used for the anode and cathode, along with the membrane, was labeled MEA0.

A fuel cell test station (Beam 100 from Beam Associate Co., Ltd.) was used to measure the polarization curves of a 5 cm^2 single-cell with a serpentine flow pattern. Hydrogen and oxygen were supplied to both the anode and cathode at 50 sccm. The performance of the MEAs was characterized at 0.56 V min^{-1} potential sweeping rate at 25 and 65 °C by the fuel cell test station. The humidified temperatures of the electrodes and MEA were kept identical, and polarization measurements were performed under ambient conditions.

3. Results and discussion

3.1. Characterization of the TiVCr coatings deposited on GDL

Fig. 1(a) and (b) show the wide-angle XRD patterns of the TiVCr-coated Si substrate and GDL at various sputtering times. As shown in Fig. 1(a), the diffraction peaks of the TiVCr coatings obtained at 10 min sputtering time are observed at 2θ values of 41.06°, consistent with the (110) crystalline plane of the BCC crystalline structure. Both V and Cr exhibit a BCC structure, whereas Ti is BCC at 1150 K, which could be retained at room temperature by alloying with a small amount of certain elements, such as Nb or V [23]. Thus, the TiVCr alloy coatings form a single BCC structure, similar to that reported by Tsai et al. [19]. As the sputtering time increases to 60 min, the intensity of the (110) peak increases significantly and shifts to a larger 2θ value of 41.75°. This result is attributed to differences in the stoichiometry of the TiVCr alloy caused by the different sputtering yields of the element in the alloy. The

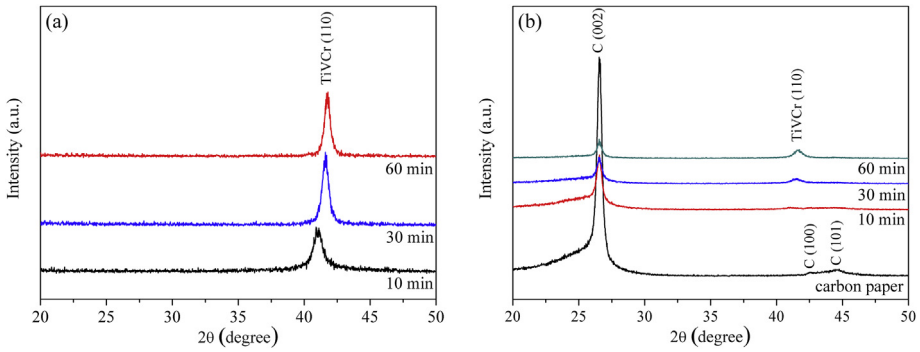

Fig. 1. Wide-angle XRD patterns of the TiVCr coatings on (a) Si substrates and (b) GDLs obtained at various sputtering times.

diffraction pattern of the TiVCr-coated GDL is shown in Fig. 1(b); while the peaks observed are similar to those of the TiVCr-coated Si substrate, the preferred orientation is different.

Fig. 2 shows plain-view and cross-sectional SEM micrographs of the TiVCr-coated Si substrates obtained at various sputtering times. A pyramid-like appearance and columnar microstructure are present in the substrate obtained at a sputtering time of 10 min [Fig. 2(a)]. The pyramidal protrusions feature sizes ranging from 33 nm to 67 nm. When the sputtering time is increased to 30 min [Fig. 2(b)], the surface pyramidal protrusions become more compact and their sizes range from 50 nm to 117 nm. At 60 min of sputtering [Fig. 2(c)], the V-shaped columnar structure with a clearly faceted surface becomes very distinct, coinciding with the good crystallinity and preferred (110) orientation observed in previous XRD analyses. The pyramidal protrusions exhibit surface sizes ranging from 58 nm to 150 nm. The coating thickness of the

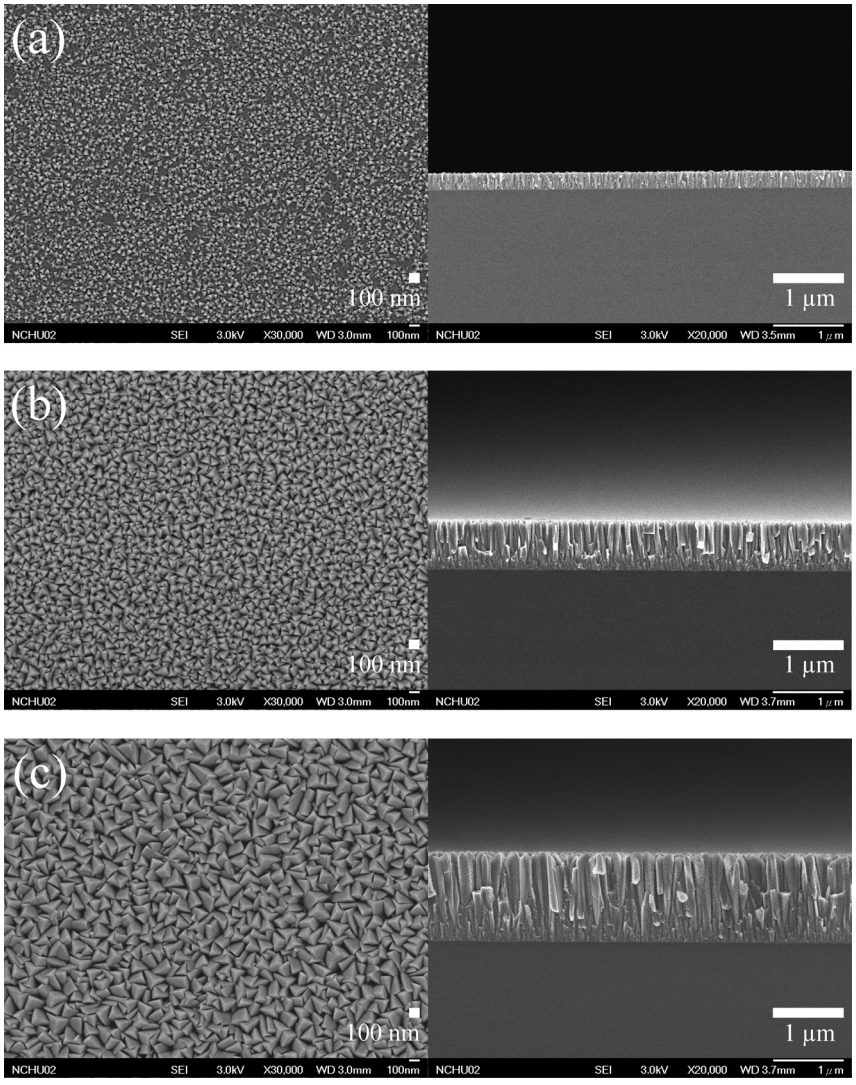

Fig. 2. Plain-view and cross-sectional SEM micrographs of TiVCr-coated Si substrates obtained at sputtering times of (a) 10, (b) 30, and (c) 60 min.

TiVCr thin films increases to 248, 722, and 1280 nm as the sputtering time increases to 10, 30, and 60 min, respectively. Fig. 3 shows plain-view and cross-sectional SEM micrographs of TiVCr-coated GDLs obtained at different sputtering times. The morphology of the TiVCr coating on the GDLs is similar to that of the Si substrates. As shown in Fig. 3(a), the surface of the carbon fibers in the GDLs is completely covered by pyramidal protrusions at a sputtering time of 10 min. The SEM micrographs show that the TiVCr coating is thoroughly coated onto the GDL and maintains a pyramidal morphology and columnar microstructure. As shown in the inset of Fig. 3, the coating thickness increases with the sputtering time.

Table 2
Ti, V, and Cr contents in the TiVCr coatings on the GDLs.

GDL samples	Ti (ppm)	V (ppm)	Cr (ppm)
TiVCr-10 m	1.376	0.934	0.918
TiVCr-30 m	1.861	2.249	2.208
TiVCr-60 m	4.071	4.877	4.754

To understand the composition and stoichiometry of the TiVCr thin films, the Ti, V, and Cr contents of the TiVCr coatings at various sputtering times were determined (Table 2) using ICP-AES. The elemental content in each coating increases with increasing

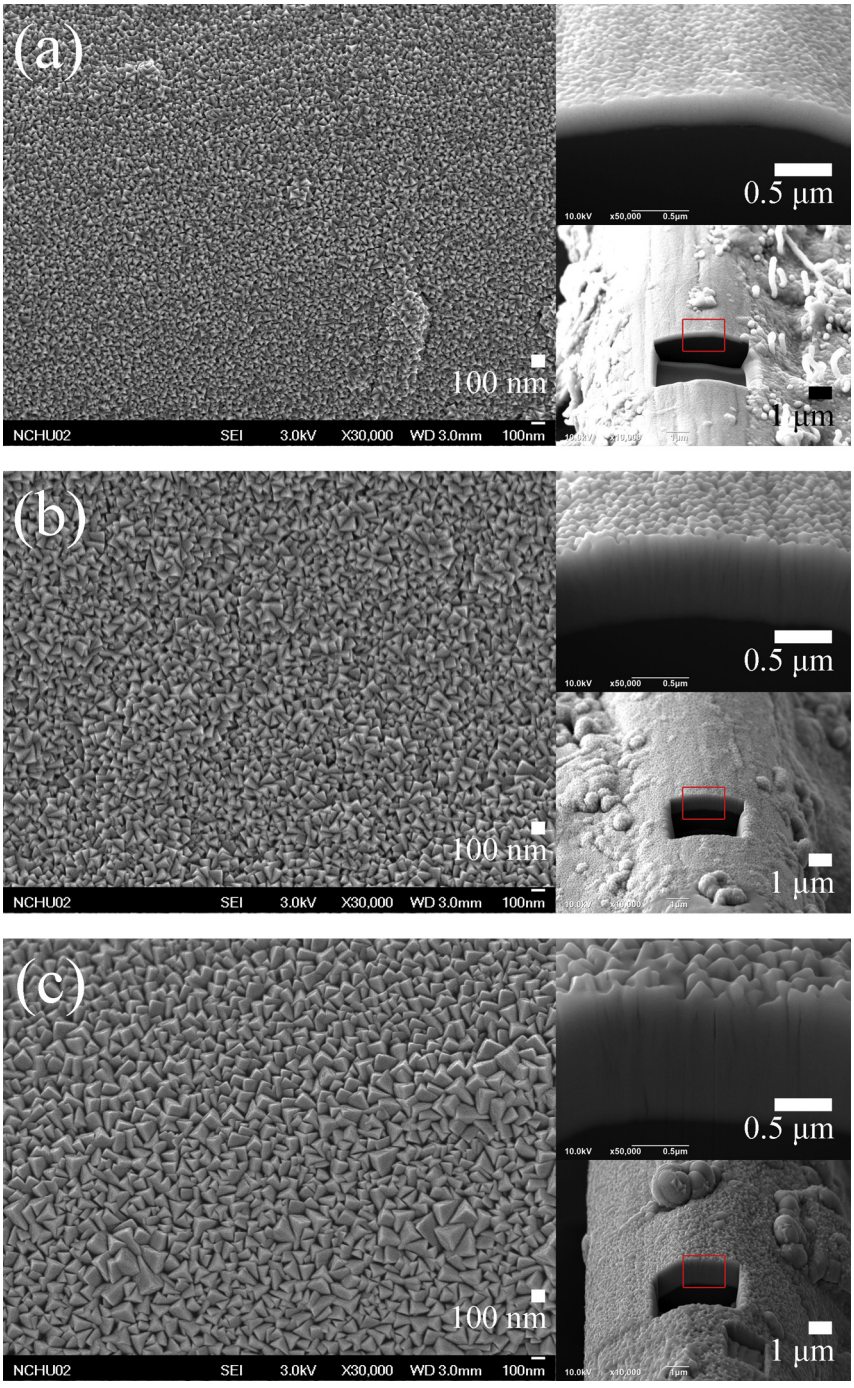

Fig. 3. Plain-view and cross-sectional SEM micrographs of TiVCr-coated GDLs obtained at sputtering times of (a) 10, (b) 30, and (c) 60 min.

sputtering time. In contrast to observations at 10 min of sputtering, the concentrations of V and Cr are higher than that of Ti at 30 and 60 min of sputtering. This result could be correlated with the diffraction peak shift found during XRD analysis.

3.2. Hydrophilicity of the TiVCr coatings on GDL

The hydrophilic characteristics of the TiVCr-coated GDL were investigated to understand the wettability of the TiVCr coating on GDL. Fig. 4 shows the images of water droplets on the GDLs with TiVCr coatings. The average water contact angles of TiVCr-10 m, TiVCr-30 m, and TiVCr-60 m are 46.02°, 34.14°, and 12.14°, respectively. The water contact angle decreases with increasing sputtering time of the TiVCr coatings. The wettability of the TiVCr-coated GDLs considerably differs from that of the as-received GDL, and this property is strongly dependent on the amount of TiVCr coating available. The result is similar to that in our previous studies, wherein a catalyst layer was added to AB_2-type hydrogen storage alloy, TiO_2, and γ-Al_2O_3 particles [24–26].

3.3. Single-cell durability test

To estimate the durability of the MEA with TiVCr-coated GDLs, after cell activation, typical current density versus time curves of the MEA operated at 0.6 V were recorded without hydrogen flow (Fig. 5). The lifetimes (durability) of the MEAs show the order MEA60 > MEA30 > MEA10 > MEA0. This result indicates that the MEAs with TiVCr coating feature improved cell durability under the absence of hydrogen flow, likely because of the hydrogen-storing characteristics of the coating. In addition, cell durability increases with increasing sputtering time of the TiVCr coatings. MEA60 presents the longest lifetime, exhibiting 90.6% longer lifetime than MEA0 (without TiVCr coating).

3.4. Single-cell polarization test

Fig. 6(a) and (b) show the polarization curves of four MEAs at 25 and 65 °C cell temperatures. Table 3 lists the corresponding maximum current density and the power density for the MEAs. The cell and humidified temperatures of both electrodes were kept constant during the experiments. Fig. 6(c) and (d) show the corresponding polarization curves over the current density range of 0.0–0.3 A cm^{-2} (activation region). In this region, the electrochemical activity of the MEAs dominantly affects the polarization curve. As illustrated in Fig. 6(c) and (d), the current densities obtained at 0.6 V cell voltage and 25 and 65 °C cell temperatures show the order MEA10 > MEA0 > MEA30 > MEA60. This result demonstrates that the hydrogen-storing characteristics of the TiVCr alloy could assist the activity of hydrogen and increase the electrochemical reaction between the GDL and the catalyst layer. Thus, MEA performance is improved at each operation condition. Among the MEAs studied, MEA10 exhibits the best performance at operating temperatures of 25 and 65 °C. These results indicate that the performance of TiVCr coatings in MEAs is determined by an optimal thickness and large surface area.

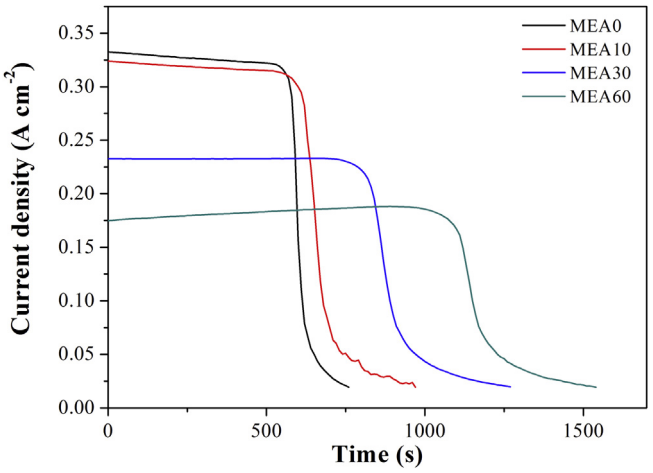

Fig. 5. Current density–time profiles of MEA operated at 0.6 V without hydrogen flow.

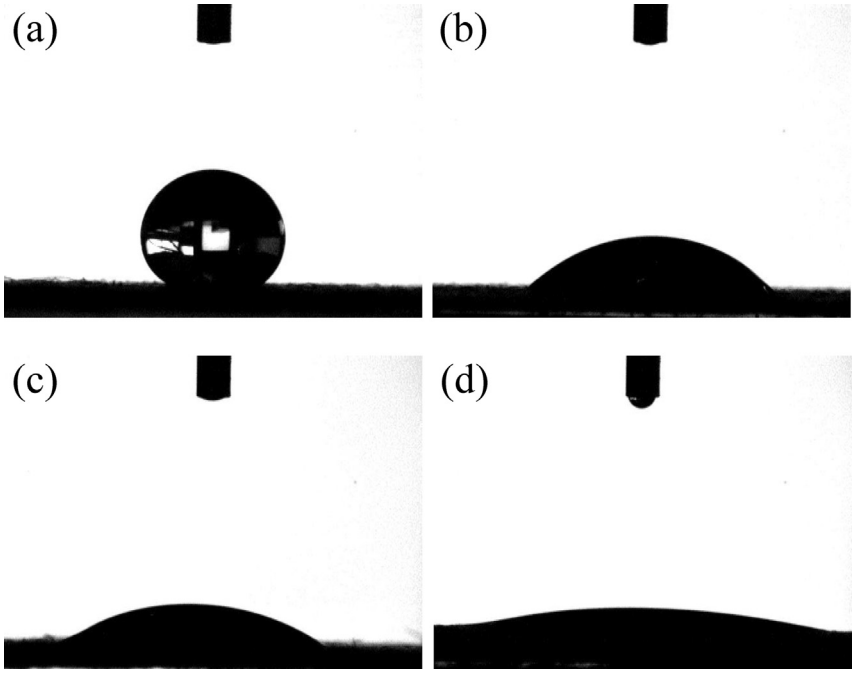

Fig. 4. Contact angle measurements using water droplets on the GDLs: (a) As-received, (b) TiVCr-10 m, (c) TiVCr-30 m, and (d) TiVCr-60 m.

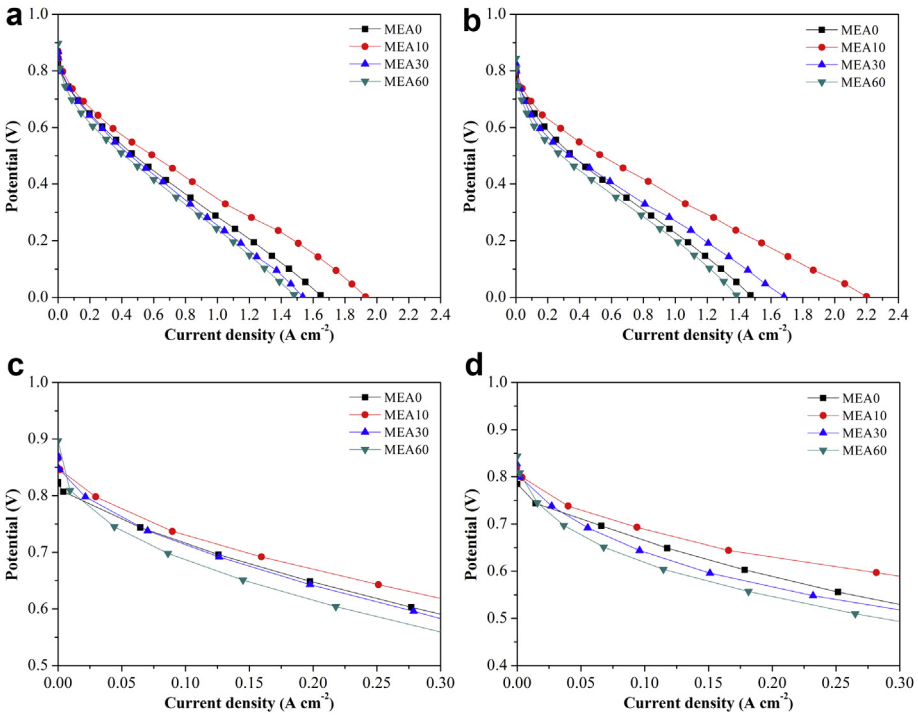

Fig. 6. Polarization curves of MEAs measured at (a) 25 and (b) 65 °C; (c) and (d) show the corresponding polarization curve plots in the current density regime from 0.0 cm^{-2} to 0.3 A cm^{-2} at 25 and 65 °C, respectively.

The SEM micrographs and ICP-AES analysis results demonstrate that the grain size, film thickness, and TiVCr coating content increase with increasing sputtering time. Despite these characteristics, however, the number of electrochemical reaction sites between the GDL and catalyst layer in the anode does not increase accordingly, which could affect electron collection. These contradictory trends result in non-uniform enhancement of the cell performance with increasing thickness of the TiVCr coatings.

The current density at cell voltages below 0.6 V is mainly affected by ohmic and concentration polarization losses. The current densities obtained at voltages below 0.6 V show the order MEA10 > MEA0 > MEA30 > MEA60 at 25 °C and MEA10 > MEA30 > MEA0 > MEA60 at 65 °C [Fig. 6(a) and (b)]. The operating temperature at 25 °C is close to non-humidification conditions. The cell performance is controlled by electrochemical reactions of the MEA. Therefore, the result of the current density at cell voltages below 0.6 V is similar to that at cell voltages above 0.6 V. At higher hydration levels, the wettability of the anodic catalyst layer is improved. The performances of MEA10 and MEA30 under full-humidification (65 °C), which are 1.87 and 1.46 A cm^{-2}, respectively, are higher than that of MEA0 at 0.1 V. Thus, the TiVCr coating assisted in absorbing water from the external humidification to achieve enhanced hydration in the MEA. As the saturation vapor pressure of water increases rapidly above 50 °C, the amount of water in the anode at a humidifier temperature of 65 °C is much greater than that at 25 °C. Water contact angle measurement results demonstrate that MEA60 features optimal hygroscopic ability. The higher water molecule absorbability of MEA60 is most likely due to blockage of the movable route of fuel in the anode GDL by the overflow of water, which deteriorates the reaction rate and cell performance.

The cell performance of the TiVCr-coated GDL is mainly determined by a competition mechanism. At non-humidification conditions, the positive effect is caused by an increase in electrochemical reaction sites between the GDL and catalyst layer and the negative effect is attributed to a decrease in the surface area of the excessively sputtered TiVCr coatings on the GDL. At humidification conditions, the positive effect arises from enhanced wettability through water absorption from the external humidifier to the anodic catalyst layer and the negative effect may be attributed to water flooding induced by excessively sputtered TiVCr coatings. The internal cell resistance is influenced by the electrochemical activity, electrical resistance, and wettability of the MEA. For further understanding, the semi-empirical equation given by Tu et al. [27], Equation (I), was adopted to estimate the internal resistance of the single-cell from the polarization curves.

Table 3
MEA performances obtained under different operating temperatures.

Operating temperature (°C)	MEA sample	Anode	Maximum current density (A cm^{-2})	Maximum power density (W cm^{-2})
25–25–25	MEA0	As-received GDL	1.647	0.292
	MEA10	TiVCr-10 m	1.929	0.346
	MEA30	TiVCr-30 m	1.535	0.274
	MEA60	TiVCr-60 m	1.481	0.262
65–65–65	MEA0	As-received GDL	1.472	0.245
	MEA10	TiVCr-10 m	2.201	0.352
	MEA30	TiVCr-30 m	1.681	0.272
	MEA60	TiVCr-60 m	1.383	0.229

$$E = A - B \times \ln i - R \times i \quad \text{(I)}$$

$$E_{\text{cell}} = E_r^o - \eta_{a,\text{act}} - \eta_{c,\text{act}} - \eta_{iR} - \eta_{a,\text{conc}} - \eta_{c,\text{conc}} \quad \text{(II)}$$

where R is the internal cell resistance. $R \times i$ denotes the internal resistance over-potential as given by η_{iR} in Equation (II), and B is the overall Tafel slope. $B \times lni$ is equivalent to the electrode activation over-potential ($\eta_{a,\text{act}} + \eta_{c,\text{act}}$) in Equation (II), and A is a constant that depends on E_r^o and the exchange current density. The presumable values of electrode resistance were obtained by a curve fitting from the set of cell potential (E) and current (i) data. Fig. 7 shows the calculated Tafel slope of the MEAs versus sputtering time of the TiVCr coatings. The Tafel slopes show the order MEA10 < MEA0 < MEA30 < MEA60 at non-humidification conditions (25 °C). This result indicates that the improved electrochemical activity of the anode decreases the electrode activation overpotential upon sputtering of the TiVCr coatings for 10 min. The Tafel slope increases dramatically with increasing TiVCr coating thickness at non-humidification conditions. Excessively sputtered TiVCr coatings on GDL decrease the number of electrochemical reaction sites between the GDL and catalyst layer, which results in an increase in the electrode activation overpotential. At full-humidification conditions (65 °C), the Tafel slopes show the order MEA10 < MEA30 < MEA0 < MEA60. The Tafel slope of MEA30 is lower than that of MEA0 at full-humidification conditions, which suggests that the hydrogen oxidation reaction occurs easily because of the improved wettability of the anode with the TiVCr coating by the external humidifier. The Tafel slope of MEA60 increases remarkably, which is very likely due to flooding.

Fig. 8 shows the calculated internal resistance of the MEAs versus the sputtering time of the TiVCr coatings. The internal resistance of MEA10 with TiVCr coating for 10 min is lower than that without the TiVCr coating at non-humidification conditions (25 °C). This observation can be ascribed to the improved activation overpotential of the anode with the TiVCr coating. The internal resistance increases thereafter because of the decrease in number of electrochemical reaction sites between the GDL and catalyst layer brought about by the excessively sputtered TiVCr coatings on the GDL. In addition, increasing the roughness of the coating, the electrical contact resistance between the coated GDL and catalyst layer may increase, which then increases the cell internal resistance. At full-humidification conditions (65 °C), the optimal sputtering time for the TiVCr coatings is mainly determined by a balance between the wettability of the catalyst layer and the

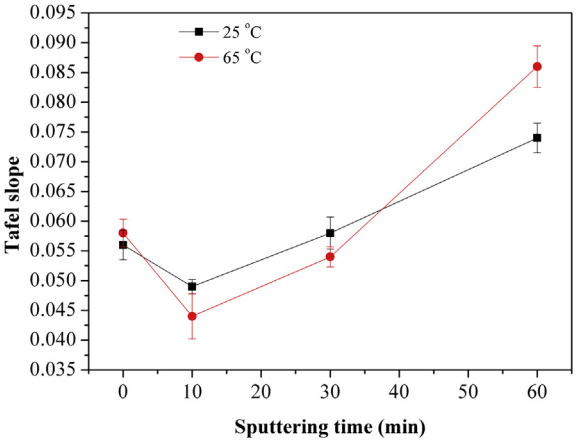

Fig. 7. Tafel slope vs. sputtering time curves obtained at different operating temperatures.

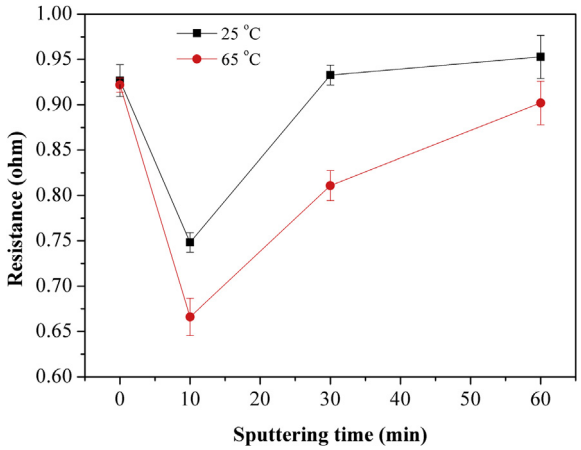

Fig. 8. Internal resistance vs. sputtering time curves obtained at different operating temperatures.

flooding phenomenon at the anode, which poses a significant influence on the internal resistance of the cell. MEA10 exhibits the lowest internal resistance among the MEAs. Thus, the appropriate water absorbability of the MEA can decrease both ionic and internal resistances. Excess water is absorbed by the TiVCr coating on the GDL in MEA60, which causes the flooding phenomenon at the anode and deteriorates cell performance.

In summary, MEA10 shows the highest power density among the MEAs at an operating temperature of 25 °C; the power density of MEA10 is 18.49% higher than that of MEA0. At 65 °C, the maximum power density of MEA10 is 43.67% higher than that of MEA0. These results clearly demonstrate that coating the anodic GDL of an MEA with an appropriate TiVCr yields enhanced cell performance.

4. Conclusion

TiVCr coatings with a pyramid-like surface feature and a typical columnar structure were deposited on GDLs by magnetron sputtering. The XRD patterns obtained confirm the BCC crystal structure of the TiVCr coatings. The Ti, V, and Cr contents in the TiVCr-coated GDL increased with increasing sputtering time. The water contact angles of the TiVCr-coated GDLs decreased with increasing sputtering time, which indicates that the hydroscopic ability of the TiVCr coating improves with time. MEA60 exhibited the longest cell lifetime at zero hydrogen flow rate, yielding a lifetime about 90.6% higher than that of MEA0 without the TiVCr coating. Among the MEA specimens studied, MEA10, which was obtained under a sputtering time of 10 min, displayed maximum power densities of 0.346 and 0.352 W cm^{-2} at operating temperatures of 25 and 65 °C, respectively; these densities are 18.49% and 43.67% higher than that of MEA0 without the TiVCr coating. Application of a TiVCr coating on the GDL of PEMFCs improves cell performance and durability.

References

[1] O.J. Murphy, G.D. Hitchens, D.J. Manko, J. Power Sources 47 (1994) 353.
[2] S. Takenaka, H. Matsumori, H. Matsune, E. Tanabe, M. Kishida, J. Electrochem. Soc. 155 (2008) B929.
[3] R. Beneito, J. Vilaplana, S. Gisbert, Int. J. Hydrogen Energy 32 (2007) 1554.
[4] F.K. Hsu, M.S. Lee, C.C. Lin, Y.K. Lin, W.T. Hsu, J. Power Sources 219 (2012) 180.
[5] J.M. Moore, J.B. Lakeman, G.O. Mepsted, J. Power Sources 106 (2002) 16.
[6] P. Agnolucci, J. Power Sources 32 (2007) 4319.
[7] X.H. Wang, Y. Chen, H.G. Pan, R.G. Xu, S.Q. Li, L.X. Chen, C.P. Chen, Q.D. Wang, J. Alloys Compd. 293-295 (1999) 833.
[8] W.K. Hu, D. Noréus, J. Alloy. Compd. 356-357 (2003) 734.

[9] Y. Chen, C. Sequeira, T. Allen, C.P. Chen, J. Alloys Compd. 404–406 (2005) 661.
[10] F. Fang, Y. Li, Q. Zhang, L. Sun, Z. Shao, D. Sun, J. Power Sources 195 (2010) 8215.
[11] G.G. Libowitz, A.J. Maeland, Mater. Sci. Forum 31 (1988) 177.
[12] E. Akiba, H. Iba, Intermetallics 6 (1998) 461.
[13] K. Kubo, H. Itoh, T. Takahashi, T. Ebisawa, T. Kabutomori, Y. Nakamura, E. Akiba, J. Alloys Compd. 356–357 (2003) 452.
[14] H. Arashima, F. Takahashi, T. Ebisawa, H. Itoh, T. Kabutomori, J. Alloys Compd. 356-357 (2003) 405.
[15] S.W. Cho, C.N. Park, J.H. Yoo, J. Choi, J.S. Park, C.Y. Suh, G. Shim, J. Alloys Compd. 403 (2005) 262.
[16] H. Itoh, H. Arashima, K. Kubo, T. Kabutomori, K. Ohnishi, J. Alloys Compd. 404–406 (2005) 417.
[17] D.C. Tsai, Y.L. Huang, S.R. Lin, S.C. Liang, F.S. Shieu, Appl. Surf. Sci. 257 (2010) 1361.
[18] D.C. Tsai, Y.L. Huang, S.R. Lin, D.R. Jung, F.S. Shieu, Appl. Surf. Sci. 257 (2011) 3969.
[19] D.C. Tsai, F.S. Shieu, S.Y. Chang, H.C. Yao, M.J. Deng, J. Electrochem. Soc. 157 (2010) K52.
[20] D.C. Tsai, S.C. Liang, Z.C. Chang, T.N. Lin, M.H. Shiao, F.S. Shieu, Surf. Coat. Technol. 207 (2012) 293.
[21] D.C. Tsai, Y.L. Huang, S.R. Lin, D.R. Jung, F.S. Shieu, Nucl. Instrum. Methods Phys. Res. Sect. B 269 (2011) 685.
[22] D.C. Tsai, Y.L. Huang, S.R. Lin, D.R. Jung, S.Y. Chang, F.S. Shieu, J. Alloy. Compd. 509 (2011) 3141.
[23] A.J. Maeland, G.G. Libowitz, J.F. Lynch, J. Less Common Met. 104 (1984) 361.
[24] W.K. Chao, L.C. Chang, R.H. Huang, K.L. Hsueh, F.S. Shieu, J. Electrochem. Soc. 157 (2010) A1262.
[25] W.K. Chao, R.H. Huang, C.J. Huang, K.L. Hsueh, F.S. Shieu, J. Electrochem. Soc. 157 (2010) B1012.
[26] W.K. Chao, C.M. Lee, D.C. Tsai, C.C. Chou, K.L. Hsueh, F.S. Shieu, J. Power Sources 185 (2008) 136.
[27] H.C. Tu, Y.Y. Wang, C.C. Wan, K.L. Hsueh, J. Power Sources 159 (2006) 1105.